JOURNAL OF MATERIALS SCIENCE 31 (1996) 513–518

Surface characterization of natural graphite powder composite electrodes by atomic force microscopy

J. FOURNIER, H. MÉNARD
Département de chimie, Université de Sherbrooke, Sherbrooke (Québec), J1K 2R1 Canada
L. BROSSARD
Institut de recherche d'Hydro-Québec (IREQ), 1800 montée Ste-Julie, Varennes (Québec), J3X 1S1 Canada
Y. JUGNET
Centre ESCA de NanoAnalyse et Technologie de surface (CENATS), 43 boulevard du 11 novembre 1918, F69622, Villeurbanne, Cédex, France

Graphite powder electrodes bonded by polymerized $LaPO_4$ have been investigated for the first time by atomic force microscopy (AFM). The interest in investigating this material stems from the fact that graphite electrodes intercalated, or not, with various metals and bonded with $LaPO_4$ have shown very good mechanical and electrochemical stability during the hydrogen evolution reaction (HER) in 1 M KOH aqueous solutions. Examination of their surfaces by scanning electron microscopy has revealed that these electrodes are very porous. AFM furnishes additional data about the surface and can therefore be considered a powerful tool for surface characterization.

1. Introduction

Since its invention in 1985, atomic force microscopy (AFM) has been presented as a new technique for obtaining high-resolution surface topography [1]. Like its predecessor, the scanning tunnelling microscopy (STM) [2], AFM is a powerful tool for this purpose but it has a major advantage over STM in that it also allows atomic resolution of non-conductive surface materials [3–4]. Its signal is generated by variations in the force between the tip and the local surface under examination [5].

So far, the investigation of graphite by STM was done mainly on highly-oriented pyrolytic graphite (HOPG). Work on other layered materials has similarly focused on single or quasi-crystals, particularly in work involving high-resolution, i.e. atomic-scale images. While single crystals offer the obvious advantage of possessing macroscopically planar and highly ordered surfaces, however, they are neither common nor readily prepared forms of most solid electrodes.

A few authors have described STM analyses of graphite in forms other than HOPG, e.g. kish (single crystal) graphite [6], flakes [7] and fibres [8]. Recently, Zhang *et al.* [9] achieved atomic resolution on pressed graphite powder (SP1 grade, 99.999% with an average particle diameter of 100 μm) a conductive material which allows a tunnelling current to flow.

In the case of materials containing an insulating binder, such as carbon paste electrodes of the Adams type in which various hydrocarbons are used as binding substances, STM clearly discriminates spatial variations of conductive and insulating regions on surfaces. Wang *et al.* [10] have characterized the microdistribution of these regions for such electrode materials as a function of the concentration of Nujol oil but obtained no information about the insulating regions, which appear as "black holes".

As far as electrochemistry is concerned, the application of scanning probe microscopy (SPM) has focused on *in situ* monitoring of redox reactions, plating, electrofinishing and other electrochemical processes on very flat surfaces (HOPG, Au, Pt etc.) [11, 12]. For industrial applications, however, it is the investigation of rough or porous materials that is more important. The particles, in pellets of such materials, commonly exhibit a strong preference toward orientation with the basal plane parallel to the pellet surface, as shown by X-ray powder diffraction studies. Recently, pelletized graphite powder electrodes in which the particles were bonded with lanthanum phosphate polymer, were characterized for the hydrogen evolution reaction (HER) in 1 M KOH [13]. It was observed that the electrode material is extremely porous. Microcrystalline graphite powders with mean particle sizes in the 40–80 μm range contain crystalline faces with ordered regions that are much larger than the scale of the AFM experiment. On the basis of these considerations, there seems to be no reason why AFM images cannot be readily obtained on pellets pressed from these powders. The present paper is devoted to further surface characterization of electrodes by AFM,

© 1996 Chapman & Hall

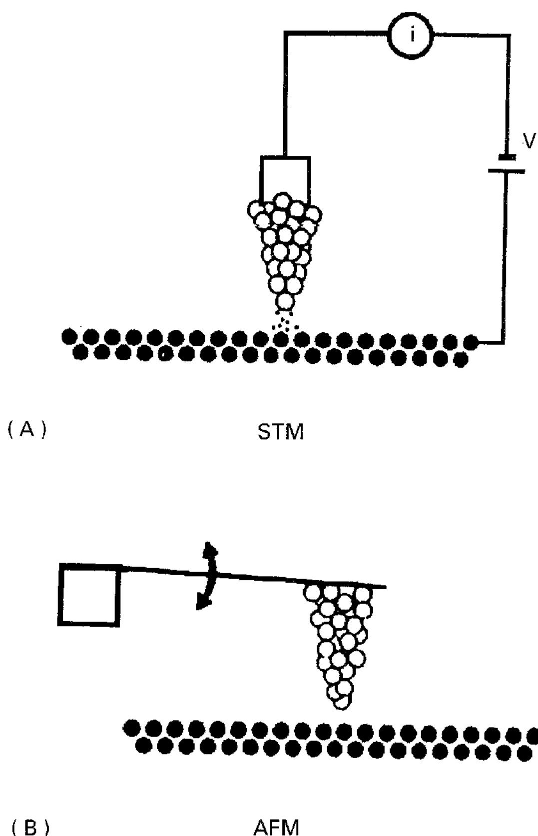

Figure 1 Schematic representation of STM (A) and AFM (B).

thereby illustrating its usefulness as a new investigating tool.

2. General considerations

Scanning tunnelling microscopy consists of measuring the tunnelling current between a polarized sharp tip located a few nanometres away from the surface under investigation (Fig. 1). Application of a potential difference between the tip and the surface with a sufficiently small gap between the two, generates a tunnelling current whose dependence on the distance, between the tip and the sample, d, is given by the relationship

$$I \propto e^{-2d/S_0} \quad (1)$$

where S_0 is the characteristic height of the "cloud" of electrons surrounding the tip and the sample. However, the tunnelling current depends not only on the distance between the tip and the sample but also on the number of electrons available in the "cloud" i.e. the nature of the atoms involved. The surface may be examined in two different ways: (i) in constant-height mode, where the current variations are monitored during the surface scan, and (ii) in constant-current mode, where the current is kept at the same value with the aid of a feedback circuit and the tip motion is recorded during a surface scan.

In STM, the tip exerts a substantial force on the sample surface through the atoms at its apex, a force of the same order of magnitude as the interatomic forces. In AFM, on the other hand, the tip is located at end of a flexible microcantilever which is deformed by the forces generated in reaction to the forces acting on the tips. The deformation induces a signal, which is recorded during a scan. Again two modes of operation are possible: (i) constant-force mode, which a feedback circuit moves the tip (or sample) forward and backward to keep the distance between the tip and the sample practically constant, and (ii) non-contact mode in which the tip is moved in a plane while recording the variations of the signal.

From the above considerations, it can be seen that STM requires a conductive material and relatively flat samples while AFM can image both conductive and non-conductive materials regardless of their surface roughness.

3. Experimental procedure

Natural graphite was used to prepare the $C/LaPO_4$ electrodes. The binder was prepared by combining acid lanthanum phosphate and lanthanum hydroxide [14].

A powder of $La(H_2PO_4)_3 + 2\,La(OH)_3$ was mixed thoroughly with natural graphite in a ratio of 1:1 wt. Approximately 1 g of the resulting powder was pressed in a mould under vacuum at a pressure of 7040 kg cm^{-2}. The polymerization reaction was carried out under argon by heating the pellets for 4 h at 400 °C. The overall polymerization reaction involved is

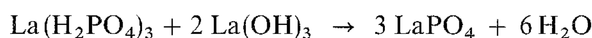

$$La(H_2PO_4)_3 + 2\,La(OH)_3 \rightarrow 3\,LaPO_4 + 6\,H_2O$$

Scanning electron microscope (SEM) images were obtained on a Jeol JSM-840A. The AFM measurements were made on a commercially available NanoScope II scanning probe microscope. The AFM was operated in constant-force mode and all scans were performed at ambient conditions.

4. Results and discussion

Fig. 2 is a close-up of the graphite electrode surface obtained by SEM which shows very clearly that this material is rough and contains pores. The white spots (indicated by arrows) correspond to $LaPO_4$ which, since it is non-conductive, causes the resistivity of the electrode material; the higher the $LaPO_4$ content, the

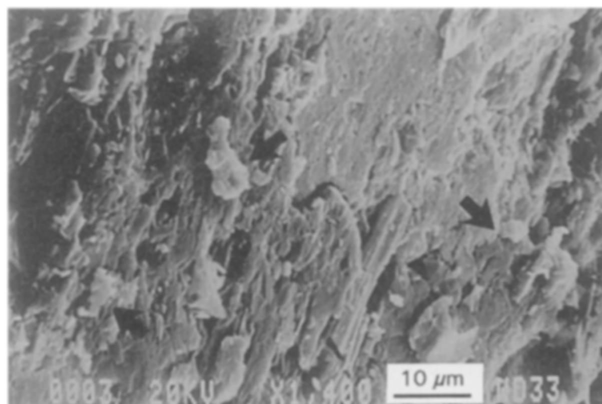

Figure 2 Large-scale view of the graphite composite electrode surface obtained by SEM (× 1400, 20 kV, WD33).

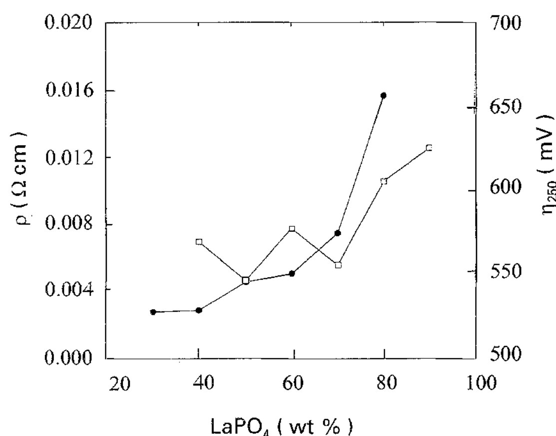

Figure 3 ● Resistivity (ρ) and □ overpotential (η) for HER in 1 M KOH at 250 mA cm^{-2} of the carbon/$LaPO_4$ electrodes as a function of the $LaPO_4$ content.

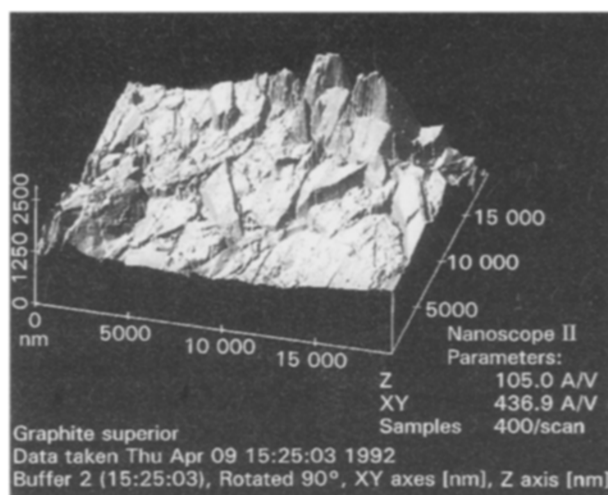

Figure 4 Large-scale AFM view of the graphite composite (50 wt % $LaPO_4$) electrode surface obtained in constant force-mode.

greater the resistivity (Fig. 3). The surface is therefore a mixture of non-conductive and conductive regions. Because of the regions with poor conductivity due to the presence of $LaPO_4$ or impurities such as sulphur or silica in the natural graphite used, enlargement with SEM reaches a limit close to 50 000 × magnification (for non-metallized surfaces) but AFM is not deterred by non-conductive regions and allows larger magnification of the electrode surface.

A graphite powder electrode surface with 50 wt % $LaPO_4$ for the bulk material is seen in Fig. 4; the image was obtained with the AFM technique in constant-force mode. The graphite particles were observed to be generally oriented in such a way that their basal plane is almost parallel to the pellet surface as reported for pelletized pure graphite [9] except that the material bond with $LaPO_4$ had more particles with their edge plane parallel to (or growing from) the surface, as illustrated in the top right corner of Fig. 4. his tendency to present a disordered surface after pressing, which can be explained by the presence of $LaPO_4$, provides key information as far as the electrochemical behaviour for the HER is concerned since the electrochemical characteristics of graphite electrodes are quite different for edge and basal planes [15–17].

Fig. 3 shows the resistivity of electrodes measured by the four point method for different $LaPO_4$ concentrations in the pellet. The resistivity increases slightly from 30 to 60 wt % $LaPO_4$ and substantially from 60 to 80 wt % owing to the non-conductive nature of $LaPO_4$. The same figure contains the η_{250} versus $LaPO_4$ concentration curve, where η_{250} is the corrected hydrogen overpotential obtained for the HER in 1 M KOH for a current of 0.250 A cm^{-2} at 25 °C. The shape of this curve suggests that the electrocatalytic activity of the electrode material for the HER is possibly related to two parameters: (i) the surface disorder tends to increase with the $LaPO_4$ content since the latter is associated with greater exposure of edge planes, which tends to promote the electrochemical activity, (ii) since $LaPO_4$ is non-conductive and non-catalytic, the electrocatalytic activity should decrease with a higher $LaPO_4$ content.

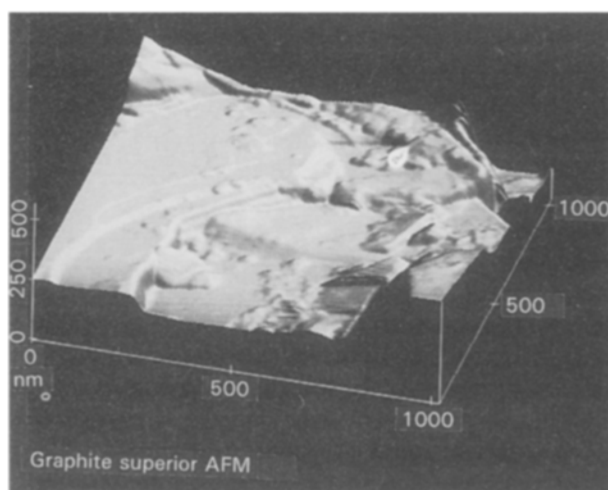

Figure 5 AFM image of the composite (50 wt % $LaPO_4$) electrode surface.

For the material concerned, STM is ineffective at the scale indicated in Fig. 4 for two reasons. Firstly, the constant-height mode cannot be used because the surface is too porous and the tip scratches the highest points, causing tunnelling-current interruptions at cavities; secondly, the constant-current mode cannot be used because the tip may be damaged in regions where $LaPO_4$ polymer is present.

Fig. 5 clearly evidences the layered nature of the electrode material. The basal plane region appears very clearly with defined contours. The high-resolution capability of AFM coupled with a digital data acquisition system allows a detailed quantitative analysis of the surface texture, i.e. the roughness factor (R). The latter is defined as the mean value of the surface relative to the centre plane and is calculated by the following relationship

$$R = \frac{1}{L_x L_y} \int_0^{L_y} \int_0^{L_x} |f(x, y)| \, dx dy \qquad (2)$$

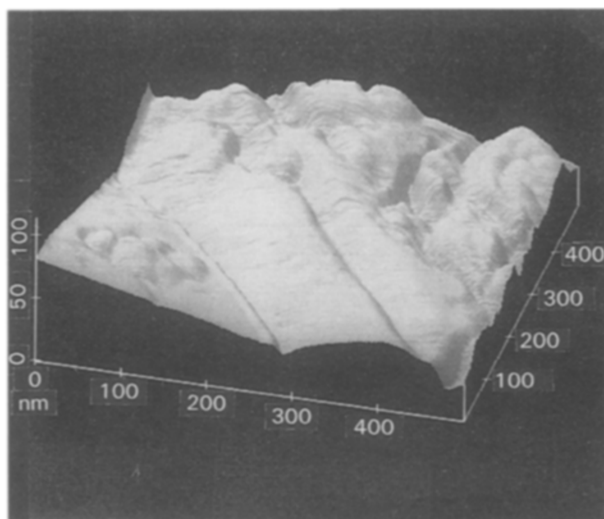

Figure 6 AFM image of the composite (50 wt % $LaPO_4$) electrode surface.

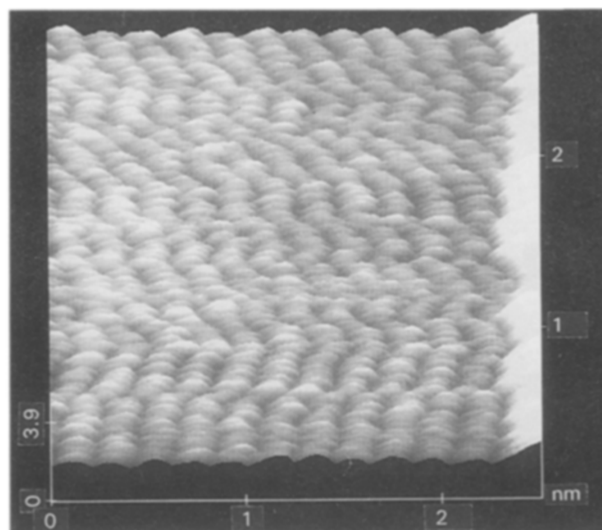

Figure 7 Atomic resolution on the composite (50 wt % $LaPO_4$) electrode surface by AFM.

where $f(x, y)$ is the surface relative to the centre plane and L_x and L_y are the dimensions of the surface. The roughness factor differs from one spot to another, with a mean value of 34.82, and depends on the surface enlargement. This can be anticipated from Fig. 6 which corresponds to the flat region of Fig. 5. R is approximately four times lower (8.366) for surface shown in Fig. 6 compared to that in Fig. 5.

AFM has two limitations for the determination of R. Firstly, it is blind for surfaces that are re-entrant, or "folded", so that the corresponding micrographs must be interpreted with care. Secondly, the tips themselves limit the resolution to which roughness can be measured, since the micrograph convolutes the surface with the tip shape.

The roughness factor is generally high for a region characterized by large differences in the height of the highest and lowest points on the surface compared to the mean plane. A relatively flat surface may also give a high value of the roughness factor when strongly inclined; in these cases, determination of the fractal dimension [18] should allow discrimination with a non-flat surface. In order to calculate the fractal dimension, a three-dimensional array of cubes is superimposed on the three-dimensional image to completely encompass the image. The cube size is varied and the number of cubes intersected by the image is recorded for each size. For a given cube size, rougher samples intersect more cells than smooth samples. The fractal dimension is defined as the slope of the line obtained by plotting the log of the cell size versus the log of the cell count. The fractal dimension increases with the microroughness, from a minimum of 2 for a perfectly flat sample to a maximum of 3 for an extremely rough sample. It was 2.048 for Fig. 5 and 2.033 for Fig. 6, which indicates that the surface was smoother in the latter case.

The search for a very flat region is interesting because atomic-scale imaging can be performed on a flat spot. Fig. 7 was obtained after image treatment. The graphite surface is composed of carbon atoms occupying unequivalent A and B sites in a hexagonal structure (Fig. 8). Batra and Ciraci [19] have shown that AFM probably responds to A atoms on graphite, whereas STM responds to B atoms. It is also relevant to note that AFM is sensitive to the total charge density in the contact region, and STM to the charge density close to the Fermi level. For an AFM image on graphite, the distance between two consecutive protrusions (assumed to be A sites) should be theoretically 0.246 nm. A value of ≈ 0.23 nm is obtained from Fig. 9. The small difference (0.23 versus 0.246 nm) can probably be explained by large atomic-scale corrugations and an irregular surface. Previously, these corrugations were explained as anomalies in the surface electronic structure and deformation of graphite surface. Albrecht and Quate [3] explain that deformations are probably caused by variations in the quality of the lever/sample contact area, which result in simultaneous imaging from multiple contact points. Moreover, for imaging natural

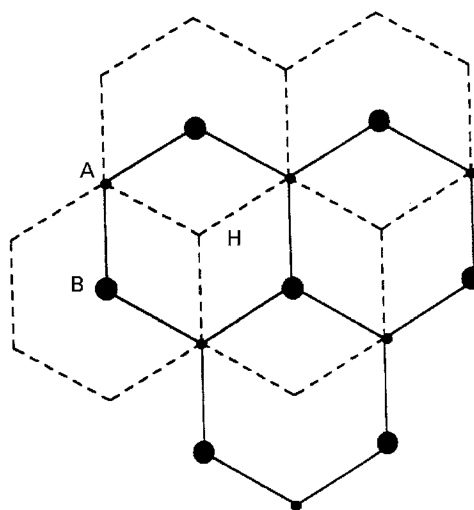

Figure 8 Two staggered layers of the (0001) graphite surface shown by solid and dotted lines. Two different (A and B) atomic sites in the top layer are indicated by small and large dots, respectively. The H site is the centre of the hexagon.

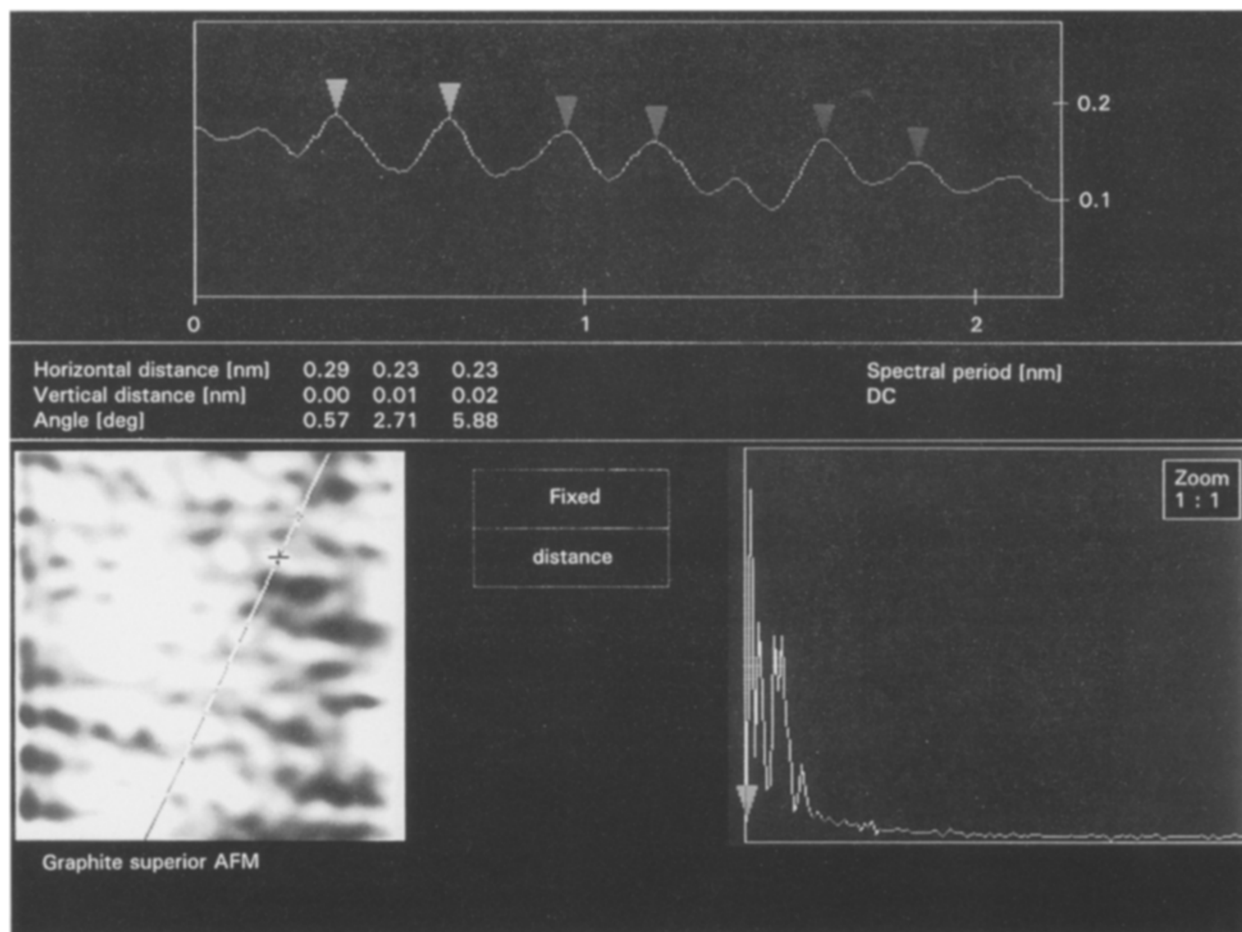

Figure 9 Parameter measurements at atomic scale on composite (50 wt % $LaPO_4$) electrode surface by AFM.

graphite in air, possible contamination of the tip [20] and relative humidity [21] must also be considered.

Surface calculations can be performed for the case illustrated in Fig. 7 where R is small (0.353) and the fractal dimension high (2.447). The values for the real surface area calculated at the scale of Fig. 7 by AFM and that by Brunauer–Emmett–Teller (BET) may be compared. The real surface area is defined as the three-dimensional area for a given projected geometric surface. In AFM, this value is the sum of the areas of the triangles formed by three adjacent data points. For Fig. 7, the real surface area is $1.50 \times 10^{-4}\ \mu m^2$ while the surface area ratio (defined as the ratio of the three-dimensional surface area to the two-dimensional surface area corresponding to the product of the length and width of the picture) is 23. BET measurements on the electrode gave 7.8 m^2 for an electrode of 1 g with a geometric surface area of 2.6 cm^2 and the surface area ratio is 30 000. This large difference cannot be explained by the limitations of AFM discussed above but is due to the fact that measurements at this scale on this particular material can only be taken on the basal planes of graphite powder. On the other hand, the active surface and the catalytic activity are strongly related to the edge planes [16].

5. Conclusion

For the first time, atomic force microscopy has been successfully used for surface characterization of graphite composite electrodes allowing the roughness factor to be calculated down to the atomic scale.

Acknowledgements

Special thanks are due to Dr Linlin Chen and Dr Daniel Guay from INRS-Énergie et Matériaux (Varennes, Canada) for help with the roughness factor calculations. The financial support of CRSNG is gratefully acknowledged.

References

1. G. BINNIG, C. F. QUATE, and CH. GERBER, *Phys. Rev. Lett.* **56** (1986) 930.
2. G. BINNIG and H. ROHRER, *Surf. Sci.* **126** (1983) 236.
3. T. R. ALBRECHT and C. F. QUATE, *J. Vac. Sci. Technol.* **A6** (1988) 271.
4. H. HEINZELMANN, E. MEYER, P. GRÜTTER, H.-R. HIDBER, L. ROSENTHALER, and H.-J. GÜNTHERODT, *ibid.* **A6** (1988) 275.
5. G. BINNIG, CH. GERBER, E. STOLL, T. R. ALBRECHT and C. F. QUATE, *Europhys. Lett.* **3** (1987) 1281.
6. S. MORITA, S. TSUKADA and N. MIKOSHIBA, *J. Vac. Sci. Technol.* **A6** (1988) 354.
7. D. P. KIM, M. M. LABES and L. M. SIPERKO, *Mater. Res. Bull.* **25** (1990) 1461.
8. J.-B. DONNET and R.-Y. QIN, *L'Actualité chimique* **2** (1992) 168.
9. Z. ZHANG, M. M. LERNER, V. J. MARTY and P. R. WATSON, *Langmuir* **8** (1992) 369.
10. J. WANG, T. MARTINEZ, D. R. YANIV, L. McCORMICK, *J. Electroanal. Chem.* **286** (1990) 265.

11. R. SONNENFELD, J. SCHNEIR and P. K. HANSMA, in "Modern aspects of electrochemistry", No. 21, edited by R. E. White, J. O'M. Bockris, B. E. Conway (Plenum Press, New York, 1990) p. 1.
12. M. M. DOVEK, M. J. HEBEN, N. S. LEWIS, R. M. PENNER and C. F. QUATE, in "Electrochemical surface science, molecular phenomena at electrode surfaces", ACS Symposium Series, edited by M. P. Soriaga (American Chemical Society, Washington, DC, 1988) p. 174.
13. J. FOURNIER, P. K. WRONA, A. LASIA, R. LACASSE, J. M. LALANCETTE, H. MÉNARD and L. BROSSARD, *J. Electrochem. Soc.* **139** (1992) 2372.
14. H. DUMONT, P. K. WRONA, L. BROSSARD, J. M. LALANCETTE and H. MÉNARD, *J. Appl. Electrochem.* **22** (1992) 1049.
15. R. L. McCREERY, in "Electroanalytical chemistry", Vol. 17, edited by A. J. Bard (Marcel Dekker Inc, New York, 1991) p. 221.
16. J. P. RANDIN and E. YEAGER, *J. Electroanal. Chem.* **36** (1972) 257.
17. P. LOS, A. LASIA, J. FOURNIER, L. BROSSARD and H. MÉNARD, *J. Electrochem. Soc.* **141** (1994) 2716.
18. Instruction manual. NanoScope II scanning probe microscope (Digital Instruments 1989).
19. I. P. BATRA and S. CIRACI, *J. Vac. Sci. Technol.* **A6** (1988) 313.
20. J. E. YAO and Y. K. JIAO, *ibid.* **A8** (1990) 508.
21. T. THUNDAT, X.-Y. ZHENG, G. Y. CHEN and R. J. WARMACK, *Surf. Sci.* **294** (1993) L939.

Received 15 April 1994
and accepted 3 February 1995